



Synthesis and characterization of Ag/AgX-CNT nanocomposites for the degradation of cyanide using visible light

E.S. Baeissa^a, R.M. Mohamed^{a,b,*}

^aFaculty of Science, Chemistry Department, King Abdulaziz University, P.O. Box 80203, Jeddah 21589, Saudi Arabia, Tel. +966 126500000; Fax: +966 2 6952292; email: redama123@yahoo.com (R.M. Mohamed)

^bAdvanced Materials Department, Central Metallurgical R&D Institute, CMRDI, P.O. Box 87, Helwan, Cairo, Egypt

Received 12 November 2015; Accepted 16 February 2016

ABSTRACT

Ag@AgCl-MWCNT nanocomposites were prepared using an *in situ* oxidation method. Different techniques, such as XPS, XRD, PI, TEM, UV-vis spectroscopy, and BET, were employed to characterize Ag@AgCl and Ag@AgCl-MWCNT nanocomposites. The analytical results demonstrated that the addition of MWCNT improved the dispersion of Ag and AgCl. The photocatalytic performance of Ag@AgCl and Ag@AgCl-MWCNT nanocomposites was studied by measuring the degradation of cyanide under visible light irradiation. The addition of MWCNT to Ag@AgCl increased the photocatalytic performance of the nanocomposites. Specifically, the photocatalytic degradation of Ag@AgCl nanoparticles was lower than that of Ag@AgCl-MWCNT nanocomposites because the addition of MWCNTs promoted the separation of electrons and holes. The degradation of cyanide by Ag@AgCl-MWCNT nanocomposites followed first-order reaction kinetics.

Keywords: Photocatalysis; Cyanide; Ag@AgCl; MWCNT

1. Introduction

Cyanide (CN) is an inorganic pollutant that is released into the aquatic environment from different anthropogenic sources. For example, cyanide is produced in various industries, such as photography, pharmaceuticals, plastics, ore leaching, metal mining, finishing, cleaning, plating, processing, electroplating, automobile parts manufacture, steel milling, steel tempering, and coal coking [1–3]. CN typically exists in several different forms, such as simple salts (KCN or NaCN and HCN) or complexes [2–8]. CNs are weakly bonded within soils and form complexes with metals such as copper, iron, zinc, and nickel, which are often found in industrial effluents and remain in the water.

CN anion and hydrogen cyanide are considered the most toxic form of cyanide. CN forms a weak acid dissociable complex with Cu, Cd, Zn, and Ni [6,7] and a strong acid dissociable complex with Au, Co, Ag, and Fe [6,7]. CNs also exist as organic compounds, such as propionitrile and acrylonitrile [9].

The concentration of cyanide in the environment primarily depends on the type of human activities. The normal cyanide level of unpolluted streams and lake waters is approximately 0.001–0.05 ppm [10]. The cyanide concentration range for regular industrial effluents is between 0.01 and 10 ppm [10], while the cyanide concentration for the industrial effluent of an electroplating plant is approximately 100,000 ppm [10]. Hence, effluents from different industries must be treated prior to release, and the minimum cyanide

*Corresponding author.

concentration of wastewater for discharge into sewers is strictly controlled in many countries. For example, the proposed limits for the total cyanide content of aquatic biota and drinking water are 50–200 ppm, respectively, according to the US Environmental Protection Agency. Likewise, German and Swiss regulations limit the cyanide concentration to 0.01 ppm for surface water and 0.5 ppm for sewer water [11].

Accordingly, cyanide removal, degradation, and/or recycling are crucial for reducing the cyanide concentration of aquatic environments to meet regulatory limitations. Therefore, before discharging into the environment, cyanide must be removed from effluent. Different treatment methods for the removal of cyanides are known, including physical removal, adsorption, complexation, and oxidation [12–14]. Alkaline chlorination is the most common technique for the removal of cyanide. However, toxic cyanogens are evolved in this process, and chlorination increases the total dissolved solids content of the water [15].

Another method of contaminant removal is the photocatalytic degradation of pollutants. When solar light is used for degradation, these methods are even more economical and widely applicable [16]. Titanium dioxide is the most common photocatalyst [17–21] because it is nontoxic and can be used many times without reducing the photocatalytic activity. Compared to conventional treatment methods, which are less efficient, the use of TiO₂ particles for the photocatalytic degradation of dyes under UV or visible light (VL) has attracted significant attention [19,20].

Nevertheless, TiO₂ is rarely used as a photocatalyst for wastewater treatment due to its low effectiveness in photodegradation [22]. Many researchers have devoted their efforts to enhance the photodegradation efficiency of TiO₂ by deposition and the use of metal dopants [23–27], which only slightly enhanced the TiO₂ photocatalytic activity or even decreased the efficiency [28]. The photocatalytic activity of ZnO or TiO₂ could be enhanced by adding adsorbents such as zeolites, clay, silica, alumina, and glass [29–34].

Currently, many studies have shown that activated carbons can be used as co-adsorbents to enhance the photocatalytic activity of TiO₂ due to their high adsorption capacity and porous structure [30–35]. Many mechanisms have been proposed to explain the removal of organic compounds by titania photocatalysts. For instance, one mechanism suggests that the degradation of organic compounds may be initiated by free radicals such as HO• [36]. In another mechanism, organic compounds adsorb on the surface of the photocatalyst, and excited superficial e⁻/h⁺ pairs or HO• radicals react with the pollutant [37]. Neverthe-

less, few studies have reported the adsorption kinetics of organic compounds on photocatalysts [38–40].

Carbon nanotubes (CNTs) have attracted the attention of scientists all over the world due to their unique 1-D structure, electronic properties, and extraordinary mechanical properties, which has enabled their use in different applications. Many advanced composites contain CNTs due to their high mechanical strength [41]. CNTs may be metallic, semi-metallic or semi-conducting, depending on the tube diameter [42], allowing their use in nanoscale electronic devices. Due to the hollow and layered structures of CNTs, as well as their large specific surface area, CNTs are excellent materials for the storage of hydrogen [43]. Moreover, CNTs have been successfully used as high efficiency adsorbents for different pollutants [44–49]; thus, CNTs are considered promising materials for environmental remediation.

Recently, considerable effort has been devoted to the design of Ag/AgX (X = Cl, Br, I) composite materials due to the surface plasmon resonance of metallic Ag [48,50–53], which can dramatically enhance the absorption of VL and provide new opportunities for the development of VLD photocatalysts [54]. For example, Ag/AgX (X = Cl, Br) [55], Ag/AgBr/TiO₂ [52,56], and Ag@AgCl grafted onto graphene sheets [57] have shown enhanced VLD photocatalytic activity for the degradation of various organic pollutants in water.

Zhang et al. developed an effective photocatalytic bacterial inactivation method using a AgBr–Ag–Bi₂WO₆ nanojunction system under VL irradiation (completely killed 5×10^7 cfu mL⁻¹ *Escherichia coli* K-12 within 15 min) [58]. Hu et al. prepared a novel Ag/AgBr/TiO₂ photocatalyst, which showed high inactivation efficiency for *E. coli* under VL irradiation [52].

However, photo-induced charge-transfer behavior limits the photoconversion efficiency, and the reusability of Ag/AgX is not acceptable [52,58]. Therefore, loading Ag/AgX onto a suitable supporting material may be an ideal solution for overcoming the above-mentioned drawbacks of this type of photocatalyst.

In the present study, different Ag@AgCl-MWCNTs were synthesized by the sol-gel technique. The prepared nanocomposites were characterized using various analytical tools and were evaluated for the photocatalytic degradation of cyanide in wastewater.

2. Experimental

2.1. Catalyst preparation

2.1.1. Materials

High purity multi-walled carbon nanotubes (MWCNTs) were purchased and used as received.

Ethylene glycol (EG), silver nitrate, anhydrous ethanol, sodium nitrate, ferric chloride, and ethanol were obtained from Sigma-Aldrich.

2.1.2. Preparation of Ag

AgNO₃ was added to 40 mL of EG, and the mixture was stirred vigorously for 10 min. The resulting solution was heated to 180°C for 2 h. Finally, the Ag nanoparticles were separated, washed with ethanol, and dried at 60°C for 8 h.

2.1.3. Preparation of Ag-MWCNT

First, 0.5 g of MWCNTs were added into 40 mL of EG, and the mixture was stirred vigorously for 10 min. The resulting solution was heated to 180°C for 2 h. AgNO₃ was added, and the mixture was stirred for 30 min. The final suspension was cooled to room temperature and was washed separately three times with water and ethanol. Lastly, the composite was dried at 60°C.

2.1.4. Preparation of Ag@AgCl-MWCNT

Ag@AgCl-MWCNT nanocomposites were synthesized using an *in situ* oxidation method. Ag-MWCNT powder was added to 20 mL of EG and was mechanically stirred for 20 min to obtain any evenly dispersed solution. Next, 5 mL of FeCl₃ (Fe:Ag = 0.9:1) was added into the solution, which was maintained at a temperature of 25°C for 10 min. Finally, the resulting precipitate was quickly centrifuged, washed, and dried at 60°C for 8 h. For comparison, Ag@AgCl was prepared according to the above method without using MWCNTs. In addition, the weight percent (wt.%) of MWCNT was varied to produce nanocomposites with different MWCNT contents, including 0, 1, 2, 3, and 4 wt.% MWCNT.

2.2. Photocatalyst characterization

A Bruker Axis D8 using Cu K α radiation ($\lambda = 1.540 \text{ \AA}$) was used to determine the X-ray diffraction patterns of Ag@AgCl and Ag@AgCl-MWCNT nanocomposites. A Nova 2000 series Chromatech apparatus was used to measure the BET surface area of Ag@AgCl and Ag@AgCl-MWCNT nanocomposites. Prior to measurement, the samples were heated under vacuum for 3 h at 200°C. A UV/Vis/NIR spectrophotometer (V-570, JASCO, Japan) was used to measure the band gap energy of Ag@AgCl and Ag@AgCl-MWCNT nanocomposites, and a JEOL-JEM-1230 microscope was used to determine the shape and par-

ticule sizes of the nanocomposites. Prior to analysis, the samples were dispersed in ethanol for 30 min, and a small portion of the samples was placed on a carbon-coated copper grid. A Thermo Scientific K-ALPHA, X-ray photoelectron spectroscope (XPS), England, was used to determine the elemental composition of the sample. Photoluminescence emission spectra were measured using a Shimadzu RF-5301 fluorescence spectrophotometer.

2.3. Photocatalytic activity

The use of the nanocomposites as catalysts for the photodegradation of cyanide was investigated under VL. The experiments were carried out using a horizontal cylinder annular batch reactor. The photocatalyst was irradiated with blue fluorescent light (150 W), and the reactor was covered with two UV filters. The intensity of the UV light was confirmed to be less than the detection limit (0.1 mW/cm²) of the UV radiometer. In a typical experiment, the catalyst was suspended in 300 mL of a potassium cyanide (KCN) solution (100 mg/L, pH 10.5, to avoid the evolution of HCN gas), which was adjusted using a solution of ammonia. The reaction was carried out isothermally at 25°C, and samples of the reaction mixture were taken at different intervals for a total reaction time of one hour. The CN_(aq)⁻ concentration of the samples was estimated by volumetric titration with AgNO₃, using potassium iodide to determine the endpoint of the titration. The removal efficiency of CN_(aq)⁻ was measured by applying the following equation:

$$\% \text{ Removal efficiency} = (C_0 - C)/C_0 \times 100 \quad (1)$$

where C₀ is the initial concentration of uncomplexed CN_(aq)⁻ in solution and C is the concentration of non-oxidized CN_(aq)⁻ in solution.

The photocatalytic reaction was carried out in the absence of irradiated light and in the presence of the photocatalyst to study the adsorption efficiency. The reaction was also repeated in the presence of irradiated light and in the absence of the photocatalyst to determine if degradation occurred due to light only. No reaction was observed due to adsorption or light only.

To study the effect of the MWCNT content on the photocatalytic performance of Ag@AgCl for the degradation of cyanide, experiments were carried out under the following conditions: KCN concentration = 100 ppm of KCN; volume of KCN solution = 500 mL; pH of KCN solution = 10.5; weight of the photocatalyst = 0.3 g; light source = visible light.

To determine the effect of the amount of Ag@AgCl-MWCNT-3 wt.% on the degradation of cyanide, experiments were carried out under the following conditions: concentration of KCN = 100 ppm; volume of KCN solution = 500 mL; pH of KCN solution = 10.5; photocatalyst = Ag@AgCl-MWCNT-3 wt.%; light source = visible light.

3. Results and discussion

3.1. Characterization of Ag@AgCl and Ag@AgCl-MWCNT nanocomposites

The XRD patterns of Ag@AgCl and Ag@AgCl-MWCNT nanocomposites are shown in Fig. 1. A peak for MWCNT was not observed due to the excellent distribution of MWCNT on the surface of AgCl or the low MWCNT content. The characteristic peak for the AgCl phase (JCPDS file, 31-1238) (27.8° , 32.3° , and 46.3°) appeared in all of the samples, and the characteristic diffraction peak of Ag (JCPDS file, 65-8428) facets at 37.8° was also detected. The characteristic peak of AgCl became broader as the weight percentage of MWCNT increased, indicating that the crystalline size of AgCl decreased with an increase in the MWCNT content.

The XPS spectra for Ag@AgCl-MWCNT-3 wt.% are shown in Fig. 2. As shown in Fig. 2(A), which displays the XPS spectra for Ag 3d, the Ag 3d spectrum consisted of two individual peaks at approximately 367.8–373.8 eV, which were attributed to the binding energies of Ag 3d_{5/2} and Ag 3d_{3/2}, respectively.

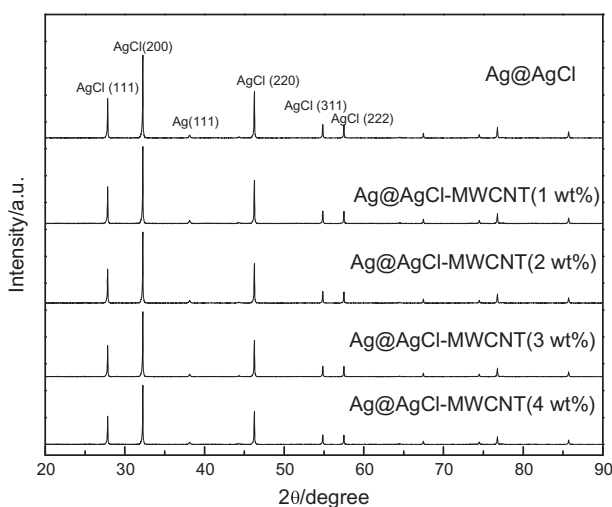


Fig. 1. XRD patterns of Ag@AgCl and Ag@AgCl-MWCNT nanocomposites with different wt.% of MWCNT.

Each peak was further deconvoluted into two peaks, yielding two doublets. The first doublet at 367.8 and 373.8 eV, which occupied a larger area, was attributed to Ag¹⁺ from AgCl, while the smaller doublet at 368.8 and 374.8 eV was assigned to metallic Ag⁰ [48,59,60]. Fig. 2(B) shows the XPS spectra for Cl 2p. Two peaks were observed at binding energies of 198.2–199.7 eV and were assigned to the characteristic doublets of Cl 2p_{3/2} and Cl 2p_{1/2}, respectively [48,59,60]. The XPS spectra for Ag 3d and Cl 2p confirmed that the obtained product consisted of metallic Ag and AgCl [48,59,60]. Fig. 2(C) shows the XPS spectra for the C1s of MWCNT and Ag@AgCl-MWCNT. The C1s XPS spectrum of Ag@AgCl-MWCNT exhibited C–O and C=O functionalities, and their peak intensities were smaller than those of MWCNT.

The TEM images of Ag@AgCl and Ag@AgCl-MWCNT are shown in Fig. 3. The results demonstrated that the dispersion of Ag@AgCl on the surface of the MWCNTs increased as the wt.% of MWCNT increased from 1 to 3 wt.%, as shown in Fig. 3(B)–(D). However, when the wt.% of MWCNT was greater than 3%, a significant effect on the dispersion of Ag@AgCl was not observed, as shown in Fig. 3(E).

The BET surface area of Ag@AgCl and Ag@AgCl-MWCNT are shown in Table 1. The results revealed that the addition of MWCNT to Ag@AgCl increased the BET surface area. Specifically, the BET surface area of Ag@AgCl increased from 6.4 to 7.7, 8.3, 9.6, and 10.1 m²/g as the wt.% of MWCNT increased from 0 to 1, 2, 3, and 4, respectively.

Fig. 4 shows the UV–vis spectra of Ag@AgCl and Ag@AgCl-MWCNT. The results demonstrated that the absorption edges of Ag@AgCl shifted to longer wavelengths as the wt.% of MWCNT increased from 0 to 3 wt.%. However, the absorption edges of Ag@AgCl remained unchanged when the wt.% of MWCNT was greater than 3 wt.%, as shown in Fig. 4. The band gaps of Ag@AgCl and Ag@AgCl-MWCNT, which were calculated from the UV–vis spectra results, were 2.5, 2.31, 2.11, 1.97, and 1.95 eV for Ag@AgCl, Ag@AgCl-MWCNT-1 wt.%, Ag@AgCl-MWCNT-2 wt.%, Ag@AgCl-MWCNT-3 wt.%, and Ag@AgCl-MWCNT-4 wt.%, respectively.

The PL spectra of Ag@AgCl and Ag@AgCl-MWCNT are shown in Fig. 5. The results demonstrated that the PL emission intensity of Ag@AgCl decreased as the wt.% of MWCNT increased from 0 to 3 wt.%. However, the PL emission intensity of Ag@AgCl remained unchanged when the wt.% of MWCNT was greater than 3 wt.%, as shown in Fig. 5. Thus, MWCNT trapped electrons, which increased the life time of electron-hole recombination.

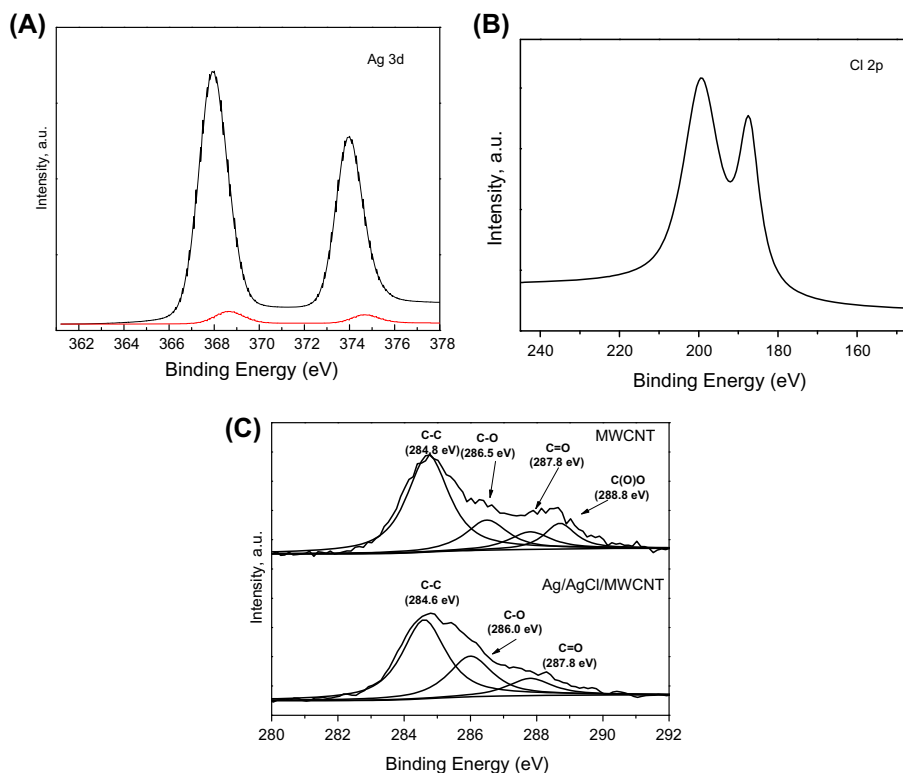


Fig. 2. XPS spectra of Ag@AgCl-MWCNT-3 wt.%: (A) Ag 3d, (B) Cl 2p, and (C) C1s.

3.2. The photocatalytic performance for the degradation of cyanide

3.2.1. Effect of the wt.% of MWCNT on the photocatalytic performance of Ag@AgCl for the degradation of cyanide

Fig. 6 shows the effect of the wt.% of MWCNT on the photocatalytic performance of Ag@AgCl. As the wt.% of MWCNT increased from 0 to 3 wt.%, the photocatalytic performance of Ag@AgCl increased from 45 to 98%, respectively. However, increasing the content of MWCNT to more than 3 wt.% did not have a significant effect on the photocatalytic performance of Ag@AgCl. To confirm the complete degradation of cyanide into CO_2 and N_2 , gases obtained from the photocatalytic process was passed through a flask containing 0.2 M sodium hydroxide, to which a solution of barium nitrate was added, leading to the formation of a white precipitate, which was examined by XRD. Fig. 7 shows the XRD pattern of the white precipitate. The results revealed that the pattern of the white precipitate were indicative of barium carbonate; therefore, carbon dioxide was one of the products obtained by the photocatalytic degradation of cyanide.

The reaction order with respect to cyanide was determined by plotting the reaction time vs. log

[cyanide] for Ag@AgCl and Ag@AgCl-MWCNT, according to the following equation:

$$\text{Log}[C]_c = -kt + \text{Log}[C]_0 \quad (2)$$

where $[C]_0$ and $[C]_t$ represent the concentration of the substrate in solution at time zero and the concentration of the substrate at the time of illumination, respectively, and k represents the apparent rate constant (min^{-1}). The apparent rate constants are summarized in Table 2. The results showed that the reaction followed first-order kinetics with respect to cyanide, and the rate constants ranged between $1,282 \times 10^{-5}$ and $3,911 \times 10^{-5} \text{ min}^{-1}$. The first-order rate equation for cyanide was expressed as: $R = k [\text{cyanide}]$. The rate of the reaction for Ag@AgCl-MWCNT-3 wt.% was approximately three times greater than that of Ag@AgCl.

3.2.2. Effect of the amount of Ag@AgCl-MWCNT-3 wt.% on the degradation of cyanide

The effect of the amount of Ag@AgCl-MWCNT-3 wt.% on the degradation of cyanide is shown in Fig. 8. As the amount of Ag@AgCl-MWCNT-3 wt.%

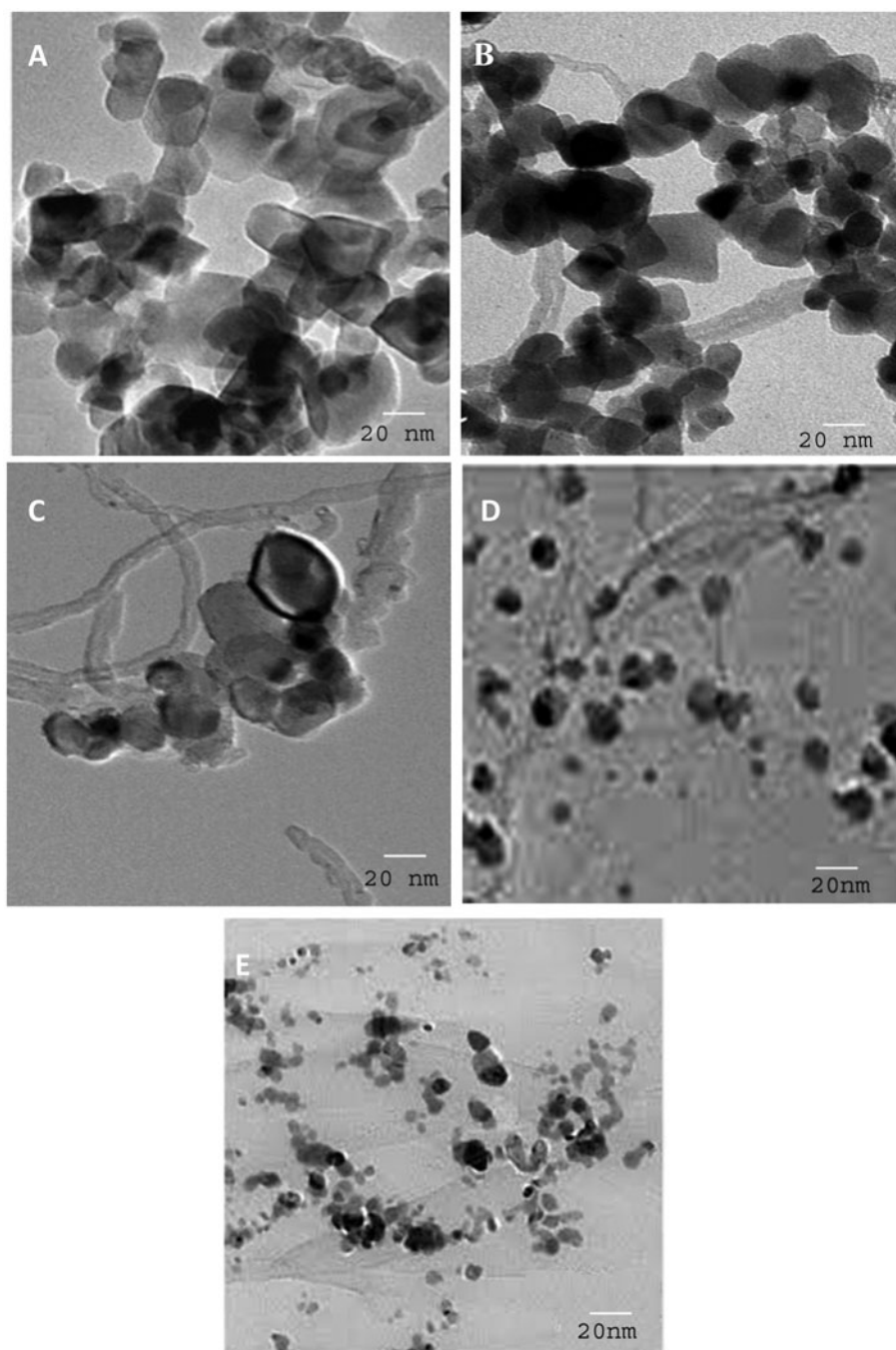


Fig. 3. TEM images of Ag@AgCl (A), Ag@AgCl-MWCNT-1 wt.% (B), Ag@AgCl-MWCNT-2 wt.% (C), Ag@AgCl-MWCNT-3 wt.% (D), and Ag@AgCl-MWCNT-4 wt.% (E).

increased from 0.3 to 0.6 g/L, the photocatalytic performance increased from 84 to 98%, respectively. Moreover, the reaction time decreased from 60 to 40 min as the amount of Ag@AgCl-MWCNT-3 wt.% increased from 0.6 to 0.9 g/L, respectively. The observed decrease in the reaction time due to an

increase in the photocatalyst rose from 0.3 to 0.9 g/L was attributed to an increase in the number of active sites, which improved the photocatalytic activity. However, when the amount of Ag@AgCl-MWCNT-3 wt.% was greater than 0.9 g/L, the reaction time increased from 40 to 60 min because the high

Table 1
BET surface area of Ag@AgCl and Ag@AgCl-MWCNT nanocomposites

Sample	S _{BET} (m ² /g)
Ag@AgCl	6.4
Ag@AgCl-MWCNT (1 wt.%)	7.7
Ag@AgCl-MWCNT (2 wt.%)	8.3
Ag@AgCl-MWCNT (3 wt.%)	9.6
Ag@AgCl-MWCNT (4 wt.%)	10.1

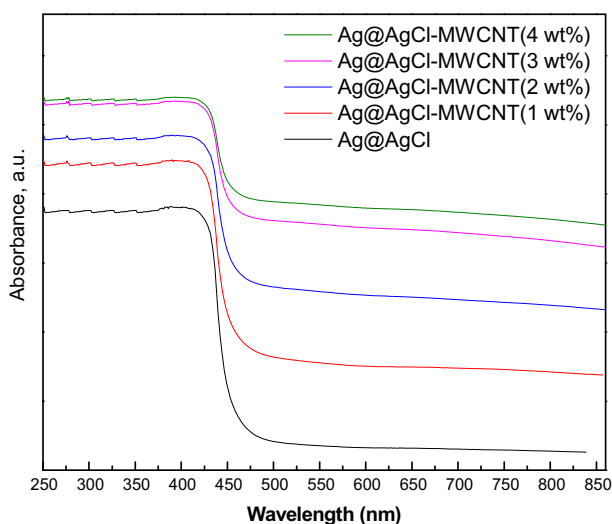


Fig. 4. UV-vis spectra of Ag@Ag Cl and Ag@AgCl-MWCNT with different wt.% of MWCNT.

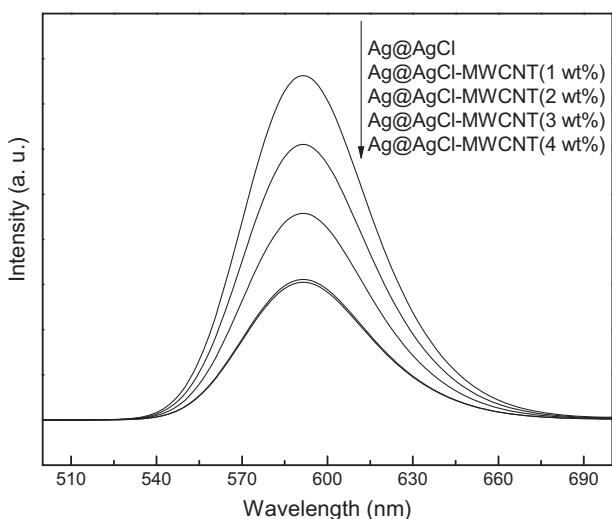


Fig. 5. PL spectra of Ag@AgCl and Ag@AgCl-MWCNT with different wt.% of MWCNT.

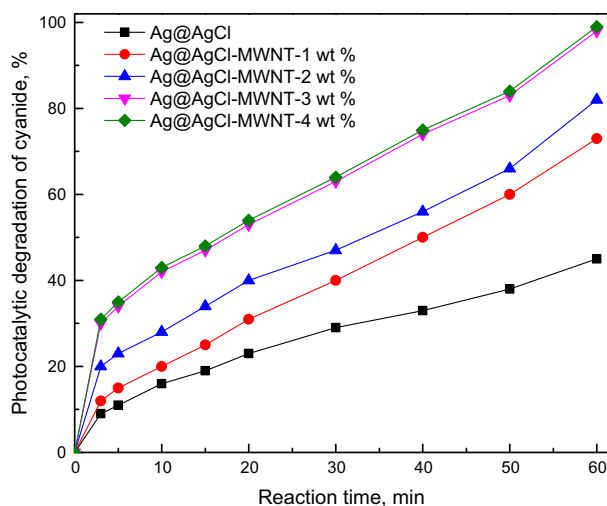


Fig. 6. Effect of the wt.% of MWCNT on the photocatalytic activity of Ag@AgCl for the degradation of cyanide.

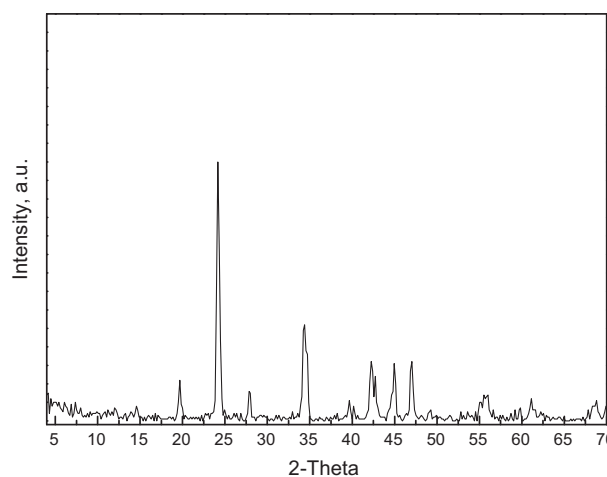


Fig. 7. XRD patterns of the white precipitate.

Table 2
Rate constant and reaction kinetics of the degradation of cyanide by Ag@AgCl and Ag@AgCl-MWCNT nanocomposites

Catalyst	$k \times 10^{-5} \text{ (min}^{-1}\text{)}$
Ag@AgCl	1,282
Ag@AgCl-MWCNT (1 wt.%)	1,838
Ag@AgCl-MWCNT (2 wt.%)	2,457
Ag@AgCl-MWCNT (3 wt.%)	3,800
Ag@AgCl-MWCNT (4 wt.%)	3,911

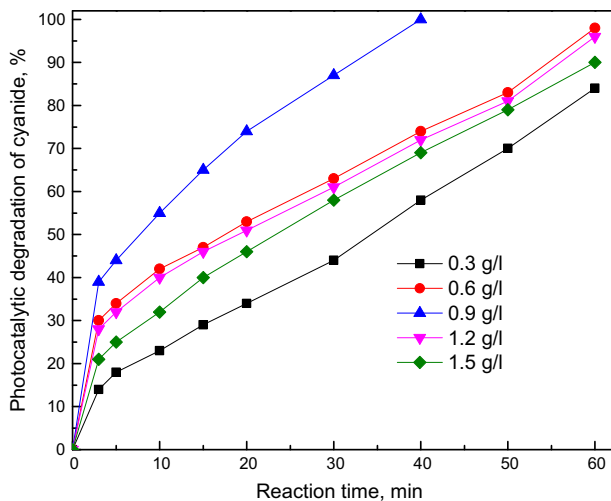


Fig. 8. Effect of the Ag@AgCl-MWCNT-3 wt.% photocatalyst content on the degradation of cyanide.

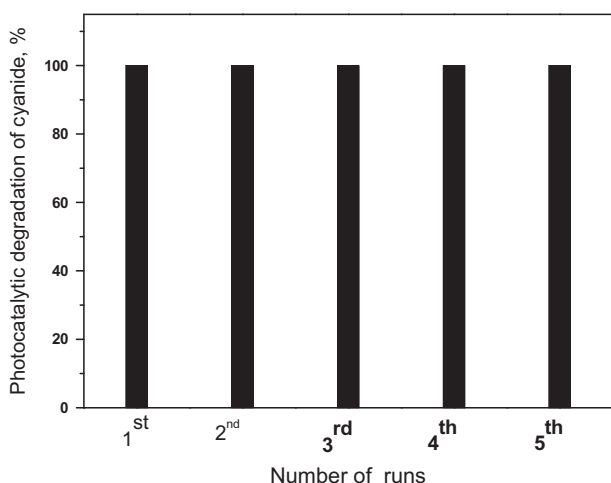


Fig. 9. The photocatalytic degradation of cyanide using Ag@AgCl-MWCNT-3 wt.% after five cycles.

photocatalyst content hindered the penetration of light to the photocatalyst surface. As a result, the reaction time increased and the photocatalytic activity decreased. Thus, the optimum amount of Ag@AgCl-MWCNT-3 wt.% was 0.9 g/L.

3.2.3. Photocatalytic stability

The photocatalytic degradation of cyanide using Ag@AgCl-MWCNT-3 wt.% after five cycles is shown in Fig. 9. The results demonstrated that the photocatalytic performance of Ag@AgCl-MWCNT-3 wt.% did not change after five runs, which indicated that Ag@AgCl-MWCNT-3 wt.% was stable after reuse.

4. Conclusions

Ag@AgCl-MWCNT nanocomposites were prepared using an *in situ* oxidation method. Different techniques, such as XPS, XRD, PL, TEM, UV-vis spectroscopy, and BET, were used to characterize Ag@AgCl and Ag@AgCl-MWCNT nanocomposites. The results demonstrated that the wt.% of MWCNT was an important parameter for controlling the BET surface area, band gap, dispersion, and particle size of Ag@AgCl. The addition of MWCNT to Ag@AgCl shifted the absorption edges of Ag@AgCl to longer wavelengths, which increased the photocatalytic performance of Ag@AgCl for the degradation of cyanide under VL. The photocatalytic performance of Ag@AgCl-MWCNT was excellent because the addition of MWCNTs enabled the trapping of photogenerated electrons, promoting electron-hole separation. Ag@AgCl-MWCNT nanocomposites showed high stability after being reused five times for the degradation of cyanide under VL irradiation.

Acknowledgments

This project was funded by Saudi Basic Industries Corporation (SABIC) and the Deanship of Scientific Research (DSR), King Abdulaziz University, Jeddah (grant number S-1436-130-6 to S-6-130-1436). Therefore, the authors gratefully acknowledge SABIC and DSR for their technical and financial support.

References

- [1] Y.M. Kim, H.U. Cho, D.S. Lee, D. Park, J.M. Park, Comparative study of free cyanide inhibition on nitrification and denitrification in batch and continuous flow systems, *Desalination* 279(1–3) (2011) 439–444.
- [2] P. Bhattacharya, S. Ghosh, A. Mukhopadhyay, Efficiency of combined ceramic microfiltration and biosorbent based treatment of high organic loading composite wastewater: An approach for agricultural reuse, *J. Environ. Chem. Eng.* 1 (2013) 38–49.
- [3] T. Depci, Comparison of activated carbon and iron impregnated activated carbon derived from Gölbaşı lignite to remove cyanide from water, *Chem. Eng. J.* 181–182 (2012) 467–478.
- [4] S. Do, Y. Jo, H. Park, S. Kong, Synthesis of iron composites on nano-pore substrates: Identification and its application to removal of cyanide, *Chemosphere* 89 (2012) 1450–1456.
- [5] M.M. Botz, Overview of Cyanide Treatment Methods, Mining Environmental Management, Mining Journal Ltd, London, UK, May 2001, pp. 28–30.
- [6] S. Ebbs, Biological degradation of cyanide compounds, *Curr. Opin. Biotechnol.* 15 (2004) 231–236.
- [7] C.M. Kao, K.F. Chen, J.K. Liu, S.M. Chou, S.C. Chen, Enzymatic degradation of nitriles by *Klebsiella oxytoca*, *Appl. Microbiol. Biotechnol.* 71 (2006) 228–233.

- [8] R.R. Dash, A. Gaur, C. Balomajumder, Cyanide in industrial wastewaters and its removal: A review on biotreatment, *J. Hazard. Mater.* 163 (2009) 1–11.
- [9] R.R. Dash, C. Balomajumder, Cyanide removal by combined adsorption and biodegradation process, *Iran. J. Environ. Health* 3 (2006) 91–96.
- [10] W.J. Rowley, F.D. Otto, Ozonation of cyanide with emphasis on gold mill wastewaters, *Can. J. Chem. Eng.* 58 (1980) 646–653.
- [11] C. Cheng, H.Y. Chen, C.S. Wu, J.S. Meena, T. Simon, F.H. Ko, A highly sensitive and selective cyanide detection using a gold nanoparticle-based dual fluorescence–colorimetric sensor with a wide concentration range, *Sens. Actuators B* 227 (2016) 283–290.
- [12] L. Sabatini, M. Battistelli, L. Giorgi, M. Iacobucci, L. Gobbi, E. Andreozzi, A. Pianetti, R. Franchi, F. Bruscolini, Tolerance to silver of an *Aspergillus fumigatus* strain able to grow on cyanide containing wastes, *J. Hazard. Mater.* 306 (2016) 115–123.
- [13] V.M. Luque-Almagro, C. Moreno-Vivián, M.D. Roldán, Biodegradation of cyanide wastes from mining and jewellery industries, *Curr. Opin. Biotechnol.* 38 (2016) 9–13.
- [14] N. Singh, B. Agarwal, C. Balomajumder, Simultaneous treatment of phenol and cyanide containing aqueous solution by adsorption, biotreatment and simultaneous adsorption and biotreatment (SAB) process, *J. Environ. Chem. Eng.* 4 (2016) 564–575.
- [15] D. Cosano, C. Esquinas, C. Jiménez-Sanchidrián, J.R. Ruiz, Use of Raman spectroscopy to assess the efficiency of MgAl mixed oxides in removing cyanide from aqueous solutions, *Appl. Surf. Sci.* 364 (2016) 428–433.
- [16] X. Yu, R. Xu, C. Wei, H. Wu, Removal of cyanide compounds from coking wastewater by ferrous sulfate: Improvement of biodegradability, *J. Hazard. Mater.* 302 (2016) 468–474.
- [17] T. Alizadeh, R.E. Sabzi, H. Alizadeh, Synthesis of nano-sized cyanide ion-imprinted polymer via non-covalent approach and its use for the fabrication of a CN⁻-selective carbon nanotube impregnated carbon paste electrode, *Talanta* 147 (2016) 90–97.
- [18] R.M. Mohamed, Mohamed Mokhtar Mohamed, Copper (II) phthalocyanines immobilized on alumina and encapsulated inside zeolite-X and their applications in photocatalytic degradation of cyanide: A comparative study, *Appl. Catal. A* 340 (2008) 16–24.
- [19] R.M. Mohamed, E.S. Baeissa, Mordenite encapsulated with Pt-TiO₂: Characterization and applications for photocatalytic degradation of direct blue dye, *J. Alloys Compd.* 558 (2013) 68–72.
- [20] F.A. Harraz, R.M. Mohamed, M.M. Rashad, Y.C. Wang, W. Sigmund, Magnetic nanocomposite based on titania–silica/cobalt ferrite for photocatalytic degradation of methylene blue dye, *Ceram. Int.* 40 (2014) 375–384.
- [21] R.M. Mohamed, E. Aazam, Synthesis and characterization of P-doped TiO₂ thin-films for photocatalytic degradation of butyl benzyl phthalate under visible-light irradiation, *Chin. J. Catal.* 34 (2013) 1267–1273.
- [22] R.M. Mohamed, UV-assisted photocatalytic synthesis of TiO₂-reduced graphene oxide with enhanced photocatalytic activity in decomposition of Sarin in gas phase, *Desalin. Water Treat.* 50 (2012) 147–156.
- [23] R.M. Mohamed, D.L. McKinney, W.M. Sigmund, Enhanced nanocatalysts, *Mater. Sci. Eng. R* 73 (2012) 1–13.
- [24] R.M. Mohamed, E.S. Aazam, Preparation and characterization of platinum doped porous titania nanoparticles for photocatalytic oxidation of carbon monoxide, *J. Alloys Compd.* 509 (2011) 10132–10138.
- [25] R.M. Mohamed, E.S. Aazam, Characterization and catalytic properties of nano-sized Au metal catalyst on titanium containing high mesoporous silica (Ti-HMS) synthesized by photo-assisted deposition and impregnation methods, *Int. J. Photoenergy* (2011), Article ID 137328, 7.
- [26] R.M. Mohamed, I.A. Mkhaliid, Characterization and catalytic properties of nano-sized Ag metal catalyst on TiO₂-SiO₂ synthesized by photo-assisted deposition (PAD) and impregnation methods, *J. Alloys Compd.* 501 (2010) 301–306.
- [27] R.M. Mohamed, I.A. Mkhaliid, The effect of rare earth dopants on the structure, surface texture and photocatalytic properties of TiO₂-SiO₂ prepared by sol-gel method, *J. Alloys Compd.* 501 (2010) 143–147.
- [28] Z.M. El-Bahy, A.A. Ismail, R.M. Mohamed, Enhancement of titania by doping rare earth for photodegradation of organic dye (Direct Blue), *J. Hazard. Mater.* 166 (2009) 138–143.
- [29] R. Saravanan, S. Karthikeyan, V.K. Gupta, G. Sekaran, V. Narayanan, A. Stephen, Enhanced photocatalytic activity of ZnO/CuO nanocomposite for the degradation of textile dye on visible light illumination, *Mater. Sci. Eng. C* 33 (2013) 91–98.
- [30] S. Joicy, R. Saravanan, D. Prabhu, N. Ponpandian, P. Thangadurai, Mn²⁺ ion influenced optical and photocatalytic behaviour of Mn-ZnS quantum dots prepared by a microwave assisted technique, *RSC Adv.* 4 (2014) 44592–44599.
- [31] R. Saravanan, M.M. Khan, V.K. Gupta, E. Mosquera, F. Gracia, V. Narayanan, A. Stephen, ZnO/Ag/Mn₂O₃ nanocomposite for visible light-induced industrial textile effluent degradation, uric acid and ascorbic acid sensing and antimicrobial activity, *RSC Adv.* 5 (2015) 34645–34651.
- [32] R. Saravanan, H. Shankar, T. Prakash, V. Narayanan, A. Stephen, ZnO/CdO composite nanorods for photocatalytic degradation of methylene blue under visible light, *Mater. Chem. Phys.* 125 (2011) 277–280.
- [33] R. Saravanan, E. Thirumal, V.K. Gupta, V. Narayanan, A. Stephen, The photocatalytic activity of ZnO prepared by simple thermal decomposition method at various temperatures, *J. Mol. Liq.* 177 (2013) 394–401.
- [34] W.D. Jing, C.M. Liu, J.L. Guo, Enhanced hydrogen production from water over Ni doped ZnIn₂S₄ microsphere photocatalysts, *Catal. Lett.* 140 (2010) 167–171.
- [35] J. Araña, J.M. Dona-Rodriguez, E.T. Rendon, C.G. Cabo, O. Gonzalez-Diaz, J.A. Herrera-Melian, J. Perez-pena, G. Colon, J.A. Navio, TiO₂ activation by using activated carbon as a support: Part II. Photoreactivity and FTIR study, *Appl. Catal. B* 44 (2003) 153–160.
- [36] B. Tryba, A.W. Morawski, M. Inagaki, Application of TiO₂-mounted activated carbon to the removal of phenol from water, *Appl. Catal. B* 41 (2003) 427–433.

- [37] J. Matos, J. Laine, J.M. Herrmann, Synergy effect in the photocatalytic degradation of phenol on a suspended mixture of titania and activated carbon, *Appl. Catal. B* 18 (1998) 281–291.
- [38] Z. Han, A. Fina, Thermal conductivity of carbon nanotubes and their polymer nanocomposites: A review, *Prog. Polym. Sci.* 36 (2011) 914–944.
- [39] K. Woan, G. Pyrgiotakis, W. Sigmund, Photocatalytic carbon-nanotube-TiO₂ composites, *Adv. Mater.* 21 (2009) 2233–2239.
- [40] Q. Li, B. Guo, J. Yu, J. Ran, B. Zhang, H. Yan, J. Gong, Highly efficient visible-light-driven photocatalytic hydrogen production of cds-cluster-decorated graphene nanosheets, *J. Am. Chem. Soc.* 133 (2011) 10878–10884.
- [41] J. Yu, T. Ma, S. Liu, Enhanced photocatalytic activity of mesoporous TiO₂ aggregates by embedding carbon nanotubes aselectron-transfer channel, *Phys. Chem. Chem. Phys.* 13 (2011) 3491–3501.
- [42] J. Yu, B. Yang, B. Cheng, Noble-metal-free carbon nanotube-Cd_{0.1}Zn_{0.9}S composites for high visible-light photocatalytic H₂-production performance, *Nanoscale* 4 (2012) 2670–2677.
- [43] A. Houas, H. Lachheb, M. Ksibi, E. Elaloui, C. Guillard, J.M. Herrmann, Photocatalytic degradation pathway of methylene blue in water, *Appl. Catal. B* 31 (2001) 145–157.
- [44] C. Wu, J. Chern, Kinetics of photocatalytic decomposition of methylene blue, *Ind. Eng. Chem. Res.* 45 (2006) 6450–6457.
- [45] G. Dai, J. Yu, G. Liu, A new approach for photocorrosion inhibition of Ag₂CO₃ photocatalyst with highly visible-light-responsive reactivity, *J. Phys. Chem. C* 116 (2012) 15519–15524.
- [46] L. Liu, J. Liu, D. Sun, Graphene oxide wrapped Ag₃PO₄ composite: Towards a highly efficient and stable visible-light-induced photocatalyst for water purification, *Catal. Sci. Technol.* 2 (2012) 2525–2532.
- [47] H. Zhang, H. Huang, H. Ming, H. Li, L. Zhang, Y. Liu, Z. Kang, Carbon quantum dots/Ag₃PO₄ complex photocatalysts with enhanced photocatalytic activity and stability under visible light, *J. Mater. Chem.* 22 (2012) 10501–10506.
- [48] Y. Hou, F. Zuo, Q. Ma, C. Wang, L. Bartels, P. Feng, Ag₃PO₄ Oxygen evolution photocatalyst employing synergistic action of Ag/AgBr nanoparticles and graphene sheets, *J. Phys. Chem. C* 116 (2012) 20132–20139.
- [49] Q. Liang, Y. Shi, W. Ma, Z. Li, X. Yang, Enhanced photocatalytic activity and structural stability by hybridizing Ag₃PO₄ nanospheres with graphene oxide sheets, *Phys. Chem. Chem. Phys.* 14 (2012) 15657–15665.
- [50] L. Ye, J. Liu, C. Gong, L. Tian, T. Peng, L. Zan, Two different roles of metallic Ag on Ag/AgX/BiOX (X = Cl, Br) visible light photocatalysts: Surface plasmon resonance and Z-scheme bridge, *ACS Catal.* 2 (2012) 1677–1683.
- [51] M.S. Zhu, P.L. Chen, M.H. Liu, Ag/AgBr/graphene oxide nanocomposite synthesized via oil/water and water/oil microemulsions: A comparison of sunlight energized plasmonic photocatalytic activity, *Langmuir* 28 (2012) 3385–3390.
- [52] C. Hu, Y. Lan, J. Qu, X. Hu, A. Wang, Ag/AgBr/TiO₂ visible light photocatalyst for destruction of azodyes and bacteria, *J. Phys. Chem. B* 110 (2006) 4066–4072.
- [53] Y. Hou, X. Li, Q. Zhao, G. Chen, C.L. Raston, Adsorption and photocatalyzed oxidation of methylated arsenic species in TiO₂ suspensions, *Environ. Sci. Technol.* 46 (2012) 4042–4050.
- [54] S. Linic, P. Christopher, D.B. Ingram, Plasmonic-metal nanostructures for efficient conversion of solar to chemical energy, *Nat. Mater.* 10 (2011) 911–921.
- [55] M.S. Zhu, P.L. Chen, M.H. Liu, Graphene oxide wrapped Ag/AgX (X = Br, Cl) nanocomposite as a highly efficient visible-light plasmonic photocatalyst, *ACS Nano* 5 (2011) 4529–4536.
- [56] Y.H. Zhang, Z.R. Tang, X.Z. Fu, Y.J. Xu, Structural characterization and photocatalytic activity of B₂O₃/ZrO₂-TiO₂ mesoporous, fibers, *Appl. Catal. B* 103 (2011) 428–435.
- [57] H.X. Shi, T.Y. Zhang, H.L. Wang, X. Wang, M. He, Photocatalytic conversion of naphthalene to α -naphthol using nanometer-sized TiO₂, *Chin. J. Catal.* 32 (2011) 46–50.
- [58] L.S. Zhang, K.H. Wong, H.Y. Yip, C. Hu, J.C. Yu, C.Y. Chan, P.K. Wong, Effective photocatalytic disinfection of *E. coli* K-12 using AgBr–Ag–Bi₂WO₆ nanojunction system irradiated by visible light: The role of diffusing hydroxyl radicals, *Environ. Sci. Technol.* 44 (2010) 1392–1398.
- [59] C. An, S. Peng, Y. Sun, Facile Synthesis of Sunlight-Driven AgCl:Ag plasmonic nanophotocatalyst, *Adv. Mater.* 22 (2010) 2570–2574.
- [60] L.H. Dong, S.S. Tang, J.Y. Zhu, P.Y. Zhan, L.F. Zhang, F.W. Tong, Photoactivated route and new bromine source for AgBr/Ag nanocomposites with enhanced visible light photocatalytic activity, *Mater. Lett.* 91 (2013) 245–248.